# $L^2$Roe: A low-dissipation version of Roe's approximate Riemann solver for low Mach numbers

K. Oßwald*, A. Siegmund**, P. Birken+,**, V. Hannemann*, A. Meister**

* DLR - Institute of Aerodynamics and Flow Technology,
Bunsenstraße 10, 37073 Göttingen, Germany.
** Universität Kassel, Institute of Mathematics,
Heinrich-Plett-Str. 40, 34132 Kassel, Germany.
+ Lunds University, Centre for the Mathematical Sciences, Lund, Sweden,
email: philipp.birken@na.lu.se.

**Abstract**

A modification of the Roe scheme aimed at low Mach number flows is discussed. It improves the dissipation of kinetic energy at the highest resolved wave numbers in a low Mach number test case of decaying isotropic turbulence. This is done by scaling the jumps in all discrete velocity components within the numerical flux function. An asymptotic analysis is used to show the correct pressure scaling at low Mach numbers and to identify the reduced numerical dissipation in that regime, both of the new method $L^2$Roe, as well as a method previously suggested by other authors. Furthermore, the analysis allows comparisons of these methods with a further low Mach scheme, LMRoe.

No conflict is observed between the reduced dissipation and the accuracy or stability of the scheme in any of the investigated test cases ranging from low Mach number potential to hypersonic viscous flow. Furthermore, a comparison with the two other methods shows advantages of the new approach.

*Keywords:* Riemann Solvers, Finite Volume Methods, Low Mach, Asymptotic Analysis, Numerical Dissipation.

## 1 Introduction

When approximate Riemann solvers were introduced into Godunov type schemes about three decades ago, an efficient way of simulating gas dynamic flows was found enabling to capture shocks within a few grid cells. In the following years many different approximate schemes were created and successfully improved to satisfy the entropy condition and handle the carbuncle phenomenon. Focusing on the schemes for perfect gas, the development of numerical flux functions was then dominated for many years by modifications to enable accurate results at low Mach numbers without loosing the stable and accurate resolution of high Mach number flow features. A particular solution to the accuracy problem at low Mach numbers for unsteady flow computations was found in the 1990s by Guillard and Viozat [8] using a preconditioning technique, which is based on the insight that the dissipation term in the numerical flux is of the asymptotically wrong order as the Mach number tends to zero. However, this scheme was subsequently shown to have stability problems [2, 4]. Therefore, different approaches have been taken in the last ten years and in particular, more analysis of the reasons for the wrong scaling has been performed. As it turns out, the problem

can be attributed to jumps in the discrete normal velocity, as was shown by analyzing Riemann problems in [7] and creation of entropy in [17]. As was shown in [12], this problem does not in fact exist on triangular grids.

For the low Mach number problem, Thornber et al. suggest a modification of the MUSCL reconstruction step [18], which changes the response of the flux function by replacing the reconstructed left and right velocities with new ones, such that the difference gets reduced with decreasing Mach number. They then show that this causes an appropriate decrease of the numerical dissipation for certain limiters, but does not solve the problem for example for van Leers limiter. A different approach is the low Mach number modification LMRoe of the Roe scheme proposed by Rieper [11]. There, only the difference in the normal velocity components is reduced within the flux function by multiplying the difference with the local Mach number in subsonic flows situations. Both of these approaches reduce the numerical dissipation, but not so much as to lead to stability problems.

As a second motivation, we consider the resolution in time of turbulent flow fields, computed via Large-Eddy Simulations (LES) or Detached Eddy Simulations (DES). This has been made possible due to the increasing computer power of recent years and exhibits a new challenge for upwind schemes. Excessive numerical dissipation in the range of higher resolved wave numbers prohibits the accurate resolution of the turbulent kinetic energy in that regime.

In this article, we therefore consider an additional modification of the LMRoe scheme for the high wave number regime corresponding to a similar reduction on the differences of tangential velocity components on top of the normal components. This new method $L^2$Roe is suitable for computations on unstructured grids with any cell type. An asymptotic analysis shows a correct scaling of the pressure at low Mach numbers, as well as a specific reduction of the numerical dissipation. Furthermore, it allows us to compare the properties of Roe, LMRoe, $L^2$Roe and the scheme of Thornber et al. in these regards. While LMRoe is based on an asymptotic analysis, the last scheme is based on less rigorous arguments. Thus, we present for the first time an analysis of that scheme, allowing us to better categorize it compared to existing approaches. The method of Thornber et al. acchieves the lower numerical dissipation via modifying the velocities, therefore changing not only the dissipative terms, but the evaluations of the physical fluxes as well. We do not consider this to be desirable, since it introduces possibly unwanted nonlinear side effects. Therefore, our method changes the numerical dissipation only.

We now first describe the governing equations and the base method, followed by the different modifications at low Mach numbers discussed here. The following section presents the asymptotic analysis. Finally numerical examples on all schemes demonstrate the range of applicability. That section culminates with the results in the case of decaying isotropic turbulence (DIT). This offers a view on the numerical dissipation of the scheme with respect to the resolved wave numbers of the flow and shows the advantage of the new approach.

Regarding notation, vectors in the coordinate space $\Re^3$ are underlined whereas bold faced variable names indicate vectors of the equation space.

## 2 Governing Equations and discretization

We first consider the compressible $d$-dimensional Euler equations

$$\begin{aligned} \partial_t \rho + \nabla \cdot \underline{m} &= 0, \\ \partial_t m_i + \sum_{j=1}^{d} \partial_{x_j}(m_i \hat{v}_j + p\delta_{ij}) &= 0, \qquad i = 1, ..., d \\ \partial_t(\rho E) + \nabla \cdot (H\underline{m}) &= 0, \end{aligned} \tag{1}$$

which model inviscid flows. Here, we have the density $\rho$, velocity vector $\underline{u} = (u_1, ..., u_d)^T$, pressure $p$ and total enthalpy $H = h + 0.5\,\underline{u} \cdot \underline{u}$. Using the vector of conservative variables $\mathbf{w} = (\rho, \rho\underline{u}, \rho E)^T$ this can be written in short as $\mathbf{w}_t + \nabla \cdot \mathbf{f}(\mathbf{w}) = \mathbf{0}$, where the Euler fluxes are given by

$$\mathbf{f}_j(\mathbf{w}) = \begin{pmatrix} \rho u_j \\ \rho u_j \underline{u} + pI \\ \rho u_j\, H \end{pmatrix}, \quad j = 1, ..., d,$$

where $I$ is the identity matrix. This system is employed for the analysis, since all the problems at low Mach numbers originate in terms present in this system.

Since we are interested eventually in viscous flows, we also consider the compressible Navier-Stokes equations in the numerical results section. For turbulent flows, either the Reynolds averaged Navier-Stokes (RANS) equations using the turbulence model of Spalart and Allmaras [14] are employed or a Large Eddy Simulation (LES) using the same turbulence model as a subgrid scale model are used, see [1] for more on these approaches.

The space discretization is a finite volume discretization, which can be written for one cell $\Omega_i$ as

$$\frac{d}{dt}\mathbf{w}_i(t) + \frac{1}{|\Omega_i|} \sum_{j \in N(i)} \sigma_{ij}(\mathbf{n}_{ij}) \mathbf{f}^{LR}(\mathbf{w}_i^+, \mathbf{w}_j^-; \mathbf{n}_{ij}) = \mathbf{0}, \tag{2}$$

where $N(i)$ constitutes the set of indices of cells neighboring cell $i$, $\Omega_i$ is the volume of that cell, $\sigma_{ij}$ the area, respectively length, of the face between cells $i$ and $j$ and $\mathbf{n}_{ij}$ the normal vector of that face pointing outwards. The numerical flux functions $\mathbf{f}^{LR}$ used here are all variants of the Roe-Pike method as described next. The values $\mathbf{w}_k^{+/-}$ are the left and right values of the numerical solution at the cell interfaces, respectively. For a first order method, these are just equal to $\mathbf{w}_k$, but for a higher order method, these will be generally different. In case that they are needed, the viscous terms are discretized using central differences.

### 2.1 Roe-Pike method

The numerical flux $f^{LR}$ of the Roe-Pike method approximating the solution of the Riemann problem between the constant states $L$ and $R$ in case of the three dimensional ($d = 3$) Euler equations can be summarized as (see e.g. [19]):

$$\mathbf{f}^{LR}(\mathbf{w}_L, \mathbf{w}_R; \mathbf{n}_{LR}) = \frac{1}{2}(\mathbf{f}_L + \mathbf{f}_R) - \frac{1}{2} \sum_{i=1}^{5} \alpha_i \, |\tilde{\lambda}_i| \, \mathbf{k}^i. \tag{3}$$

with $\mathbf{f}_L = \mathbf{f}(\mathbf{w}_L) \cdot \mathbf{n}_{LR}$ and $\mathbf{f}_R$ analogously. The wave strengths $\alpha_i$, wave speeds or eigenvalues $\lambda_i$ and eigenvectors $\mathbf{k}^i$ are given by:

$$\mathbf{k}^1 = \begin{pmatrix} 1 \\ \tilde{\underline{u}} - \tilde{a}\,\underline{n} \\ \tilde{H} - \tilde{a}\,\tilde{u}_n \end{pmatrix}, \mathbf{k}^2 = \begin{pmatrix} 1 \\ \tilde{\underline{u}} \\ 0.5\,\tilde{\underline{u}} \cdot \tilde{\underline{u}} \end{pmatrix}, \mathbf{k}^3 = \begin{pmatrix} 0 \\ \underline{t}_1 \\ \tilde{u}_{t_1} \end{pmatrix}, \mathbf{k}^4 = \begin{pmatrix} 0 \\ \underline{t}_2 \\ \tilde{u}_{t_2} \end{pmatrix}, \mathbf{k}^5 = \begin{pmatrix} 1 \\ \tilde{\underline{u}} + \tilde{a}\,\underline{n} \\ \tilde{H} + \tilde{a}\,\tilde{u}_n \end{pmatrix},$$

$$\tilde{\lambda}_1 = \tilde{u}_n - \tilde{a} \quad , \tilde{\lambda}_2 = \tilde{u}_n \quad , \tilde{\lambda}_3 = \tilde{u}_n \quad , \tilde{\lambda}_4 = \tilde{u}_n \quad , \tilde{\lambda}_5 = \tilde{u}_n + \tilde{a}\ ,$$

$$\alpha_1 = \frac{\Delta p - \tilde{\rho}\,\tilde{a}\,\Delta u_n}{2\tilde{a}^2} \ , \alpha_2 = \Delta\rho - \frac{\Delta p}{\tilde{a}^2} \quad , \alpha_3 = \tilde{\rho}\,\Delta u_{t_1} \quad , \alpha_4 = \tilde{\rho}\,\Delta u_{t_2} \quad , \alpha_5 = \frac{\Delta p + \tilde{\rho}\,\tilde{a}\,\Delta u_n}{2\tilde{a}^2}.$$

Herein $a$ denotes the speed of sound and $\underline{t}_1$ and $\underline{t}_2$ are arbitrary orthogonal unit tangential vectors spanning the plane with the normal $\underline{n}$. The velocity components in the tangential directions are $u_{t_1} = \underline{u}\,\underline{t}_1$ and $u_{t_2} = \underline{u}\,\underline{t}_2$. $\Delta$ denotes the difference between the right and left states (e.g. $\Delta p = p_R - p_L$) and $\tilde{}$ denotes the Roe averages given by:

$$\tilde{\rho} = \sqrt{\rho_L\,\rho_R}\ ;\ \tilde{\underline{u}} = \frac{\sqrt{\rho_L}\,\underline{u}_L + \sqrt{\rho_R}\,\underline{u}_R}{\sqrt{\rho_L} + \sqrt{\rho_R}}\ ;\ \tilde{H} = \frac{\sqrt{\rho_L}\,H_L + \sqrt{\rho_R}\,H_R}{\sqrt{\rho_L} + \sqrt{\rho_R}}\ ;\ \tilde{a} = \sqrt{(\gamma-1)(\tilde{H} - 0.5\,\tilde{\underline{u}} \cdot \tilde{\underline{u}})}.$$

The entropy fix of van Leer is applied on the acoustic waves ($k = 1$ and $k = 5$):

$$|\tilde{\lambda}_k|^* = \begin{cases} |\tilde{\lambda}_k| & , \quad |\tilde{\lambda}_k| \geq 2\,\widehat{\Delta\lambda_k} \\ \dfrac{\tilde{\lambda}_k^2}{4\,\widehat{\Delta\lambda_k}} + \widehat{\Delta\lambda_k}\ , & , \quad |\tilde{\lambda}_k| < 2\,\widehat{\Delta\lambda_k} \end{cases} \quad \text{with } \widehat{\Delta\lambda_k} = \max(\lambda_k^R - \lambda_k^L, 0).$$

In order to avoid shock instabilities (carbuncle phenomenon) the shock indicator proposed in [20] for the AUSMDV switch is used to locally modify the wave speed $\lambda_2$, as suggested by Liou [10]:

$$|\tilde{\lambda}_2|^* = \begin{cases} |\tilde{\lambda}_2| & , ssw_L = ssw_R = 0 \\ \max(\tilde{a}, |\tilde{\underline{u}}|) & , \text{else} \end{cases}$$

with

$$ssw_i = \begin{cases} 1\ , \lambda_1^i > 0 \text{ and } \lambda_1^j < 0 & \text{for any neighbor } j \text{ of } i \\ 1\ , \lambda_5^i > 0 \text{ and } \lambda_5^j < 0 & \text{and respective normal } \underline{n}_{ij} \\ 0\ , \text{else.} \end{cases} \tag{4}$$

# 3 Modifications at low Mach numbers

A large number of methods have been suggested to cope with the accuracy problem of classic schemes at low Mach numbers. Of these, we first present two recent ones that at the same time do not obtain an additional stability problem, before presenting our new method.

### 3.1 Modification according to Thornber et al.

Thornber et al. [18] modify the left and right velocities in order to reach the arithmetic mean of the velocities at Mach number zero:

$$\begin{aligned} \underline{u}_L^* &= \frac{(1+z)\,\underline{u}_L + (1-z)\,\underline{u}_R}{2} = \frac{\underline{u}_L + \underline{u}_R}{2} - \frac{z}{2}\Delta\underline{u} \\ \underline{u}_R^* &= \frac{(1+z)\,\underline{u}_R + (1-z)\,\underline{u}_L}{2} = \frac{\underline{u}_L + \underline{u}_R}{2} + \frac{z}{2}\Delta\underline{u} \end{aligned} \tag{5}$$

with

$$z = \min\left(1, \max(M_L, M_R)\right). \tag{6}$$

Hereby

$$M_{L/R} = \frac{|\underline{u}_{L/R}|}{a_{L/R}}.$$

are the local Mach numbers independent of the normal direction in which the flux is evaluated.

An important effect of the modification is that $\Delta\underline{u}^* = z\Delta\underline{u}$ and thus, the jumps in the velocity components are linearly reduced with decreasing Mach number. Secondary effects due to the changed velocities per se are within the nonlinear terms in the Euler flux evaluation and the difference between the arithmetic mean and the Roe averaged velocities.

Thornber et al. show that when using this in conjunction with specific high order limiters on structured grids, a numerical dissipation that is nonspurious at low Mach numbers is obtained. However, it is also shown that this is not true for the van Leer limiter.

### 3.2 LMRoe: Scaling the jump in normal velocities

The LMRoe scheme of Rieper [11] is a modification of the Roe-Pike scheme to achieve a low Mach number variant. The same linear blending function $z$ as given in equation (6) is applied within the approximate Riemann solver only on the jump $\Delta u_n$ of the normal velocity $u_n = \underline{u} \cdot \underline{n}$ which affects the wave strengths of the acoustic waves $\alpha_1$ and $\alpha_5$:

$$(\Delta u_n)^* = z\,\Delta u_n.$$

The reduction of the numerical dissipation depending on the jump in the normal component of the velocities is sufficient to improve the behavior of the scheme at low Mach numbers. However, in the vicinity of shocks small disturbances are observed. To avoid these, we suggest to use the shock indicator to keep the original scheme unmodified there:

$$(\Delta u_n)^* = \begin{cases} z\,\Delta u_n & , ssw_L = ssw_R = 0 \\ \Delta u_n & , \text{else.} \end{cases} \tag{7}$$

The indicator $ssw_{L/R}$ will be zero at low Mach numbers in the absence of shocks, thus resulting in the desired form $z\,\Delta u_n$.

### 3.3 $L^2$Roe: Decreasing the dissipation

In the asymptotic analysis performed later and the numerical results on the test case of decaying isotropic turbulence (DIT) in section 5.5, it becomes clear that the dissipation of LMRoe is still too high, whereas the method of Thornber et al. has smaller dissipation in a certain sense and

performes much better. In our view, the important difference is that in LMRoe, only the jumps in the normal components are scaled, whereas in the other method, the scaling is applied to all jumps.

However, the method of Thornber et al. acchieves this through modifying the velocities, therefore changing not only the dissipative terms, but the evaluations of the physical fluxes as well. We do not consider this to be desirable, since it introduces possibly unwanted nonlinear side effects. Therefore, we now modify LMRoe further in the spirit of changing the numerical dissipation only and no other aspects of the numerical flux function. As we will see, this will give slightly better results than the method of Thornber et al.

Thus, we apply the similar modification to both tangential components $t_1$ and $t_2$ as well, thereby reducing the numerical dissipation associated with $\mathbf{k}^3$ and $\mathbf{k}^4$ :

$$(\Delta u_t)^* = \begin{cases} z\,\Delta u_t \text{ , } ssw_L = ssw_R = 0 \\ \Delta u_t \quad \text{, else.} \end{cases} \tag{8}$$

# 4 Asymptotic Analysis

## 4.1 Pressure field

We now use an asymptotic analysis of the new scheme to show that it asymptotically obtains the correct spatial pressure distribution. For reasons of simplicity, we restrict ourselves to the two dimensional case. The nondimensional Euler equations (1) were obtained using the standard nondimensionalization which employs a pressure reference of the form $\hat{p}_{ref} = \hat{\rho}_{ref}\hat{v}^2_{ref}$. As is useful for low Mach numbers, we now employ a different nondimensionalization with a fixed pressure reference $p_{ref}$ and introduce the global Mach number

$$M = \frac{\hat{u}_{ref}}{\hat{a}_{ref}}$$

as the quotient of the reference velocity and the reference speed of sound $\hat{a}_{ref} = \sqrt{\hat{p}_{ref}/\hat{\rho}_{ref}}$. This nondimensionalization causes the factor $M^{-2}$ to appear in front of the pressure gradient. As was shown previously [8], the continuous pressure is of the form

$$p(x,t) = p^{(0)}(t) + Mp^{(1)}(t) + M^2p^{(2)}(x,t), \quad M \to 0, \tag{9}$$

meaning that the spatial variations of the pressure are on the scale of the Mach number squared. Thus, the discrete pressure should have the same property and at the core of the accuracy problem of many schemes at low Mach numbers is an asymptotically wrong spatial pressure variation.

To better understand the new method, we now repeat the basic steps of the asymptotic analysis of the Roe-Pike method for the $x$-component of the momentum update (the analysis of the $y$-component is analogous). Thus, after lengthy computations, we obtain for cell $i$ in terms of the Mach number (compare [11], appendix 2):

$$\Omega_i \frac{d}{dt}(\rho_i u_{1_i}) + M^{-2}\frac{1}{2}\sum_{l\in N(i)} p_l n_{il_x}\sigma_{il} + M^{-1}\frac{1}{2}\sum_{l\in N(i)}\left(\frac{(u_n n_x + u_1)_{il}\Delta_{il}p}{a_{il}} + \rho_{il}a_{il}n_{il_x}\Delta_{il}u_n\right)\sigma_{il}$$
$$+\frac{1}{2}\sum_{l\in N(i)}\left(\rho_l u_{1_l}\underline{u}\cdot\underline{n}_{il} - \rho_{il}|u_{n_{il}}|n_{il_y}\Delta_{il}u_t + |u_{n_{il}}|\left(\Delta_{il}\rho - \frac{\Delta_{il}p}{a^2_{il}}\right)u_{1_{il}}\right)\sigma_{il} = 0.$$

Hereby, unless it is a geometric quantity, the notation $\phi_{il}$ denotes the Roe average of $\phi_i$ and $\phi_l$.

We then expand all variables in cell $i$ in an asymptotic expansion

$$\phi(x,t) = \phi^{(0)}(x,t) + M\phi^{(1)}(x,t) + M^2\phi^{(2)}(x,t) + \mathcal{O}(M^2), \quad M \to 0. \tag{10}$$

Thus we obtain the following equations for the terms in the expansion ordered by powers of the Mach number:

$$\mathcal{O}(M^{-2}): \quad \frac{1}{2}\sum_{l\in N(i)} p_l^{(0)} n_{il_x}\sigma_{il} = 0,$$

$$\mathcal{O}(M^{-1}): \quad \frac{1}{2}\sum_{l\in N(i)} p_l^{(1)} n_{il_x}\sigma_{il} + \frac{1}{2}\sum_{l\in N(i)} \left( \frac{(u_n n_x + u_1)_{il}^{(0)} \Delta_{il} p^{(0)}}{a_{il}^{(0)}} + \rho_{il}^{(0)} a_{il}^{(0)} n_{il_x} \Delta_{il} u_n^{(0)} \right) \sigma_{il} = 0.$$

From the first equation it follows that $p_i^{(0)}$ does not vary in space, but with this and the next equation it follows that $p_i^{(1)}$ can vary in space, which contradicts the continuous analysis and explains the bad behavior of this method at low Mach numbers. Since $\Delta_{il} p^{(0)}$ vanishes, the problematic term is $\rho_{il}^{(0)} a_{il}^{(0)} n_{il_x} \Delta_{il} u_n^{(0)}$ and this is where the fix of Rieper sets in, which shifts it to a higher order of the Mach number, resulting in a method where the discrete pressure is in line with (9).

Regarding the newly proposed modification (8), we can see that firstly, $z$ will be on the order of $M$. Secondly, $ssw$ (compare (4)) will always be zero, since the flow is subsonic. Thus the implication is that when looking at a specific power of the Mach number in an asymptotic expansion of the form (10) of terms involving $\Delta_{il} u$, these terms get shifted backwards to higher powers of the Mach number. Thus, we formally have:

$$\Delta_{il} u^{(i)} = \begin{cases} \Delta_{il} u^{(i-1)}, & \text{for } i > 0 \\ 0, & \text{for } i = 0 \end{cases}. \tag{11}$$

This implies that we retain the beneficial properties of Riepers modification, since the corresponding equations of order $-1$ and $-2$ in powers of the Mach number are unchanged. Although Thornber et al. did not prove this, it becomes now clear from looking at (5) that the same is true for that method.

### 4.2 Numerical viscosity

The point where we improve upon Riepers method is the numerical viscosity. It is well known that the original Roe scheme at low Mach numbers suffers from excessive numerical viscosity. Rieper argues that a model for a numerical viscosity that is not spurious at low Mach numbers would be the equation

$$\frac{\partial}{\partial t}\phi + \frac{\partial}{\partial x}\phi = \frac{\partial^2}{\partial x^2}\phi \Delta x,$$

which is independent of the Mach number. Thus, we expect only leading order terms in the asymptotic equation containing the leading order momentum change in time. With the knowledge that for $M \to 0$ $p^{(0)}$ does not vary in space and assuming that $\rho^{(0)}$ does not vary in space, the leading order discrete $x$-momentum equation of Riepers method is

$$\Omega_i \frac{d}{dt}(\rho_i u_{1_i})^{(0)} + \frac{1}{2}\sum_{l\in N(i)} \left( \rho_l^{(0)} u_{1_l}^{(0)} \underline{u}^{(0)} \cdot \underline{n}_{il} + (\rho_{il} a_{il} n_{il_x} \Delta_{il} u_n)^{(0)} - \rho_{il}^{(0)} |u_{n_{il}}^{(0)}| n_{il_y} \Delta_{il} u_t^{(0)} \right) \sigma_{il} = 0. \tag{12}$$

In the new scheme with the additional tangential weighting (8), the last term including $\Delta_{il} u_t^{(0)}$ gets shifted to a higher order and thus the resulting leading order viscosity is

$$\phi = (\rho_{il} a_{il} n_{il_x} \Delta_{il} u_n)^{(0)} \tag{13}$$

meaning that we have reduced the numerical viscosity.

Modifying the numerical viscosity can influence stability, as was shown for the scheme of Guillard and Viozat by Birken and Meister [2]. However, in the following numerical tests no problems appeared.

Regarding the method of Thornber et al., we can apply the same argument to see that the last germ gets shifter to a higher order. However, while the remaining term (13) is formally identical, the Roe averages have been modified in their method and thus the numerical diffusion differs.

# 5 Numerical Results

All numerical results have been produced with the DLR-TAU code, which is based on a finite volume method formulated on the dual grid of a conformal mesh consisting of tetrahedra, prisms, pyramids and hexahedra [6]. Hereby, a linear reconstruction of the primitive variables is employed. A total variation diminishing (TVD) limiter is applied where needed. In particular, we employ the van Leer limiter in structured regions and a formulation based on Barth and Jesperson in unstructured parts. For turbulent flows, the Spalart-Allmaras turbulence model is employed [14].

Several tests have been conducted to demonstrate a wide range of applications. First, a supersonic, a transonic and a subsonic flow are considered to see if the modification leads to a difference in numerical results, in particular compared to the original Roe-Pike method. Then, two low Mach number cases, namely a potential flow and finally the DIT illustrate the behaviour in that regime.

## 5.1 Supersonic cylinder

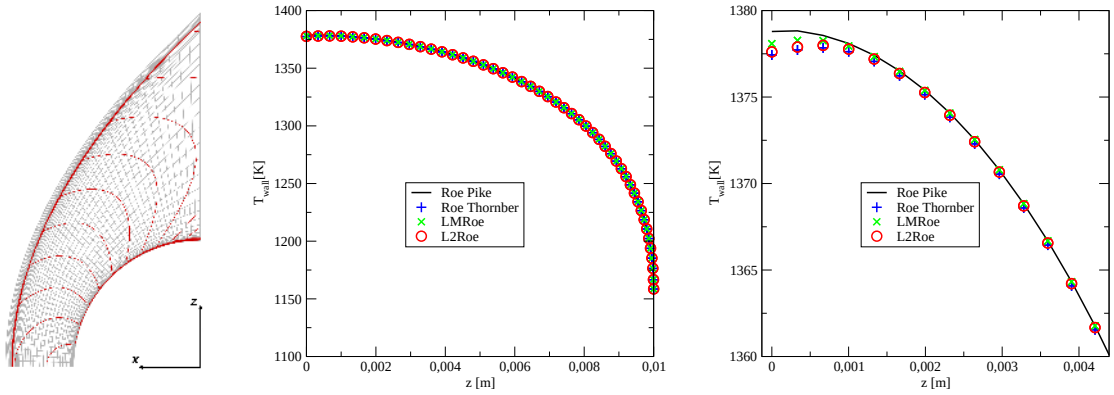


Figure 1: Mach 5 cylinder flow with radiative equilibrium at the wall; grid and Mach number isolines, $\Delta M = 0.2$ (left); wall temperature profile (middle) and close up of the stagnation region (right) over the vertical coordinate $z$.

In the first test case, a cylinder faces a Mach five flow of air ($\gamma = 1.4, R = 287\, J/(kg\, K)$) in higher atmosphere ($p_\infty = 10000 Pa, T_\infty = 250 K$), resulting in a laminar flow field. The related

Reynolds number with respect to the radius of $0.01m$ is about 138000. Hereby, the temperature dependence of the viscosity is modeled via the Sutherland formula for air:

$$\mu(T) = 17.2 \cdot 10^{-6}\, Pa\, s \left(\frac{T}{T_\infty}\right)^{\frac{3}{2}} \frac{T_\infty + 110.33\, K}{T + 110.33\, K}.$$

The heat flux $\dot{q}$ to the wall is assumed to be equal to the heat flux radiated from the wall with an emissivity $\epsilon = 0.8$ according to the Stefan-Maxwell law:

$$\dot{q} = \epsilon\, \sigma\, T_{wall}^4 \qquad \text{with } \sigma = 56.7032 \cdot 10^{-9} \frac{W}{m^2\, K^4}.$$

In Figure 1, the stable shock capturing of the new scheme and the good agreement of the wall temperatures are depicted. Similar to the other modified schemes a small drop of the profiles can be seen near the stagnation point, but all results are within 0.1%.

## 5.2 Transonic airfoil

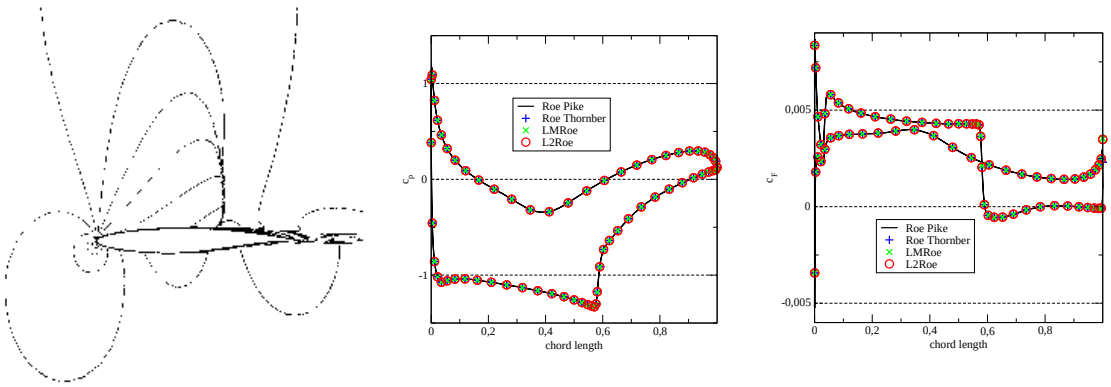


Figure 2: RAE 2822 airfoil; Mach number isolines with increments of 0.1 (left), Roe-Pike (solid line) and $L^2$Roe (dashed); pressure coefficient $c_p$ (middle) and skin friction $c_f$ (right) over the chord length, only a quarter of all surface points is depicted by a symbol.

To obtain a transonic test case, the free stream Mach number around an RAE-2822 airfoil is set at 0.75 at an angle of attack of 2.8 degree. Hereby, the Reynolds number is 6.2 million with respect to the chord length and the RANS equations are used to model the flow. The laminar to turbulent transition is set at 0.03 chord length at the upper and lower side of the airfoil's adiabatic surface. A vortex correction is applied due to the small computational domain.

The Mach number isolines are shown in Figure 2. As can be seen, the superimposed solutions of the original and modified Roe schemes are hardly distinguishable and only a small difference is present near the sharp trailing edge. The pressure coefficient as well as the skin friction do not show any significant difference.

### 5.3 Subsonic high lift airfoil

The free stream condition of the high lift configuration is a Mach number of 0.2 at an angle of attack of 20 degree and the Reynolds number is 9 million with respect to the chord length. Again, the RANS equations are used to model the flow. Slat and flap are separated from the main wing and all trailing edges have a final thickness. No vortex correction is applied due to a farfield distance of about 100 chord lengths. The wing surfaces are assumed to be adiabatic.

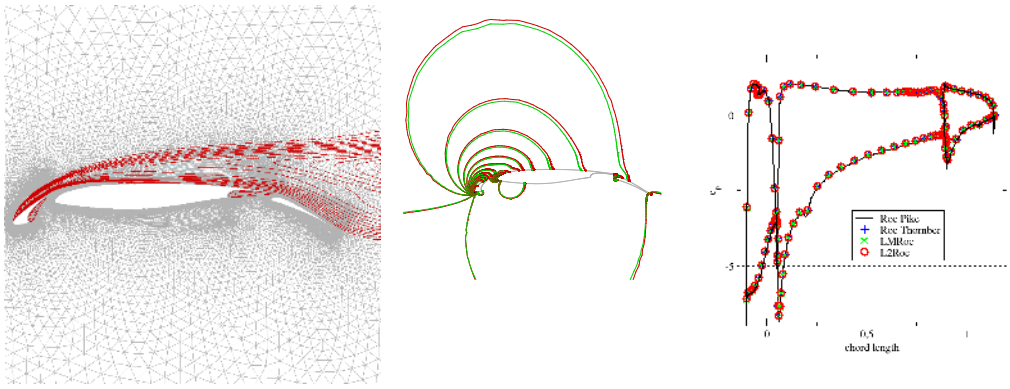


Figure 3: High lift configuration; hybrid grid with isolines of the eddy viscosity (left); pressure isolines increment of 2500 Pa (middle), Roe-Pike (red) and $L^2$Roe (green); pressure coefficient $c_p$ (right) over the chord length, only one tenth of all surface points is depicted by a symbol.

A close up of the hybrid grid around the wing is given in Figure 3 on the left. The superimposed isolines of the eddy viscosity show the predicted turbulence in the coves of the slat and the main wing as well as on the leeward side of the configuration. As expected, the wake of the slat interacts with the boundary layer on the suction side of the main wing. The pressure isolines depicted in the middle result from calculations with the Roe-Pike method (red) and $L^2$Roe (green). The qualitatively good agreement of the different formulations is quantified as pressure coefficient $c_p$ on the right. The lowest values at the suction peak on the slat are not shown in order to achieve a better scaling for the comparison along the rest of the configuration. All four solutions are close to each other even at this scale.

In the pressure distribution on the suction side all modified Roe schemes differ from the original Roe-Pike scheme, as can be seen in Figure 4 on the left and in the middle. On the right hand side of Figure 4 an enlarged view of the $c_p$ distribution at the beginning of the slat cove shows the smoother distributions of the modified schemes. The original Roe scheme has difficulties with such a low Mach number region.

### 5.4 Potential flow

In a test case with a truly low Mach number, the Euler equations are solved to simulate the inviscid flow field around a cylinder at a Mach number of $M_\infty = 0.001$. At such low Mach numbers the unmodified Roe scheme does not provide a physical solution. In the computation, the farfield boundaries are taken about 1000 cylinder diameters away from the surface. The solutions shown in Figure 5 highlight the low Mach number capability of the $L^2$Roe scheme. The other modified schemes provide similar good solutions for this case.

Notice that the benefit of the modifications is restricted to the accuracy of the converged solution and do not improve the convergence behavior of the scheme on the way to a steady state solution.

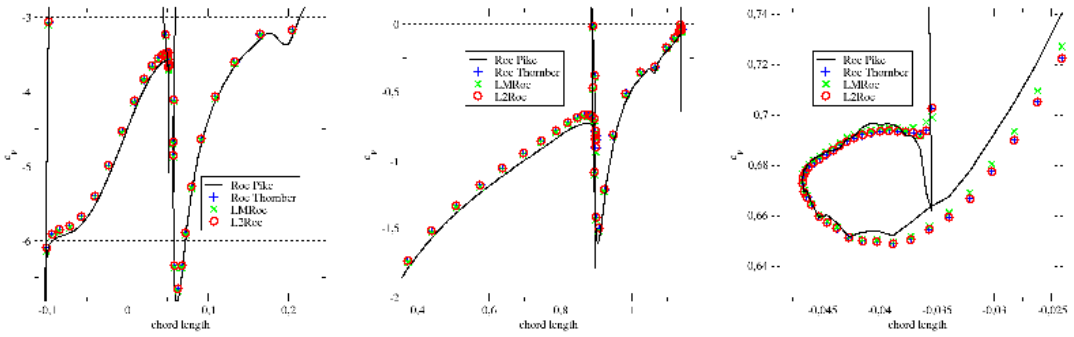


Figure 4: High lift configuration; close up views of the pressure coefficient $c_p$ over the chord length; only one tenth of all surface points is depicted by a symbol (left and middle); suction side on slat and first part of main wing (left), suction side rear part of main wing and flap (middle), first part of slat cove (right).

However, we do not observe an additional time step restriction beyond the CFL number, showing that the new scheme does not have the stability problems of for example the preconditioned Roe solver of Guillard and Viozat [2].

### 5.5 Decay of isotropic turbulence

As a last test case, decaying isotropic turbulence (DIT) is investigated on an equidistant cartesian grid. The boundary conditions are chosen to be periodic in one coordinate direction and symmetric in the other directions. Earlier tests conducted during the DESider project [9] suggest that the evolution of second order statistical moments and spectra are not influenced significantly by this choice of boundary condition as opposed to periodic boundaries on all computational domain boundaries. A second order reconstruction of the primitive variables is used without limiters due to the continuous flow field at the low Mach numbers ($M_{\max} < 0.016$). The initial velocity field is constructed to be divergence-free and to replicate the experimental kinetic energy spectra from the Comte-Bellot and Corrsin experiment [3] over all resolvable wave numbers.

The spectra measured in the experiment, as shown in Figure 6 on the left, are used as a measure to evaluate the flow solutions obtained using various numerical schemes. Note that a typical energy spectrum can be characterized by a power-law form $E(k) = C\,k^p$ where $p \approx 2-4$ in the energy-containing range, $p \approx -5/3$ in the inertial subrange and with a final range of decaying turbulence [5]. The numerical simulation should return a resolved inertial range so that the transfer of energy from large scales to smaller scales is adequately modeled within the context of LES and hybrid RANS/LES simulations. The energy transfer process is strongly dependent on the total dissipation of the numerical scheme, which can be argued to consist of three major contributions:

1. sub-grid scale (SGS) stresses,
2. molecular viscosity, and
3. the numerical dissipation of the scheme.

For the work discussed here contributions due to transport of molecular viscosity are small and the SGS model coefficient calibration has been undertaken using a central scheme with matrix

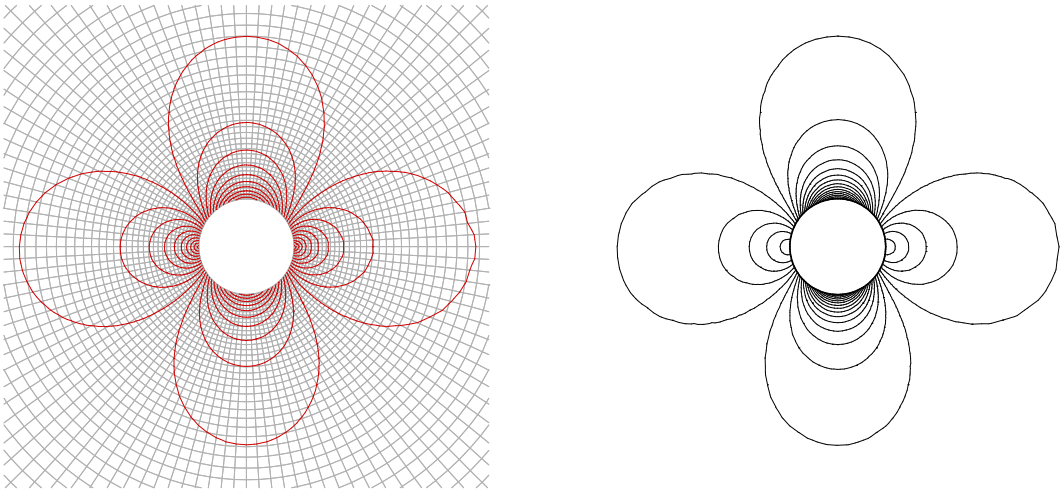

Figure 5: Inviscid flow field around a cylinder in a $M_\infty = 0.001$ flow coming from the left; grid detail and Mach number isolines (upper left); pressure isolines (upper right); horizontal velocity component (lower left); vertical velocity component (lower right).

dissipation. The Spalart-Allmaras turbulence model [14] provides our SGS model within the context of Detached Eddy Simulation [15, 16, 13]. Note that the focus of the current work is in determining the characteristics of the modified Roe scheme, so that both SGS model and molecular viscosity are kept constant throughout the investigation. The numerical dissipation of the unmodifed schemes in the high wave number regimes discussed in the paper is sufficiently strong to dominate over viscous and SGS effects.

In Figure 6 on the right, the results on a $64^3$ hexahedral grid at $t = 0.87\,\mathrm{s}$ are shown for various flux functions. Thereby, we show the numerical wave numbers for the first 31 modes, since these can be resolved on that grid. The significantly dissipative result of the original Roe scheme is representative for standard approximate Riemann solvers, whereas the improved performance of the LMRoe scheme is typical for low Mach number enhanced versions like the AUSM+up. On the contrary, the original scheme of Thornber et al. and $L^2$Roe are both resolving the energy cascade over all wave numbers on this grid. This is in line with the results of the asymptotic analysis on the numerical dissipation from section 4.2 and shows that it is worthwhile to reduce the numerical dissipation in this way. Furthermore, $L^2$Roe is slightly better on the high wave numbers than the method of Thornber et al.

We thus now concentrate on $L^2$Roe and the method of Thornber et al. The results at time $t = 2\,\mathrm{s}$ are given in Figure 7. Both show a good agreement with the experimental data with $L^2$Roe being slightly better.

The results of the present scheme on a finer mesh $128^3$ are shown in Figure 7 on the right. The improved resolution at higher wave numbers confirms the promising numerical dissipation properties of the scheme within the framework of LES or DES. In addition results achieved with the Thornber modification together with a Roe scheme underline the general applicability of the modification given in equation 5. Again the modified Roe scheme shows less dissipative results at the highest resolved wave numbers.

The same $128^3$ nodes as before are now reconnected with tetrahedral instead of hexahedral elements. Since we use a dual grid method, this leads to a polygonal grid. As can be seen, the change in the grid causes the numerical dissipation in the higher resolved wave number range to grow again as can be seen in Figure 8. The relation between the different numerical schemes is

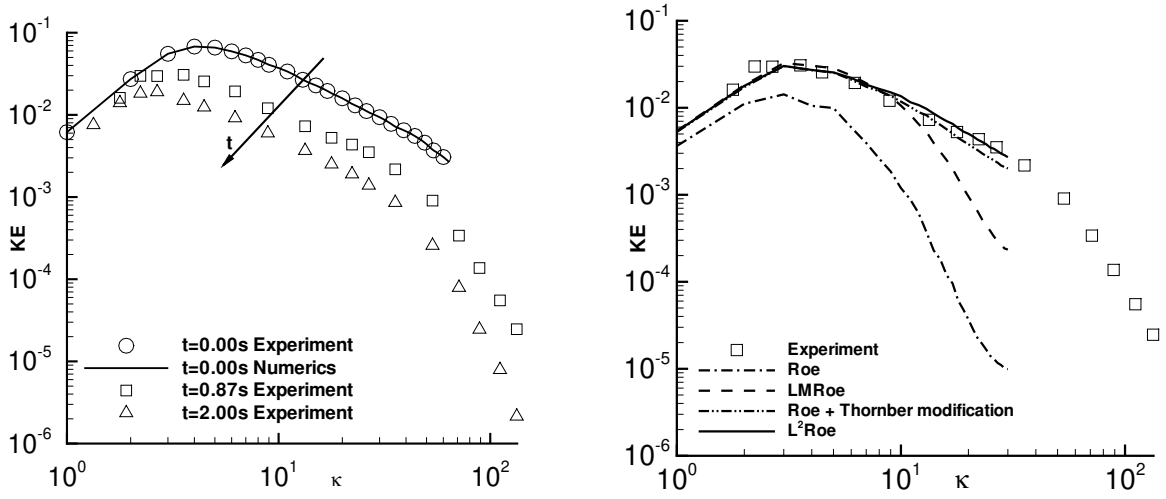


Figure 6: Turbulent kinetic energy spectra (left) at $t = 0\,\mathrm{s}$, $t = 0.87\,\mathrm{s}$ and $t = 2\,\mathrm{s}$ in the case of decaying isotropic turbulence; experimental data taken from Comte-Bellot and Corrsin [3]; numerical spectra at $t = 0.87\,\mathrm{s}$ on a $64^3$ hexahedral grid (right).

again the same: The original scheme does not give a correct solution, LMRoe a much better one and $L^2$Roe and the scheme of Thornber et al. are close with $L^2$Roe performing best. However, the value of $p$ returned in the inertial interval is significantly less than $-5/3$, implying a nonphysical high dissipation of energy.

The rotational and translational symmetry of the two grids are different. The translational offset for example is twice as large in the tetrahedral mesh compared to the hexahedral mesh. But this symmetry aspect should not deteriorate the numerical dissipation of the scheme in the higher resolved wave number range.

# 6 Summary and Conclusions

We developed a low dissipation version of the low Mach modification LMRoe [11] of Roe's approximate Riemann solver. This new method $L^2$Roe is applicable without user defined parameters for a large Mach number regime. An asymptotic analysis shows that the method complies with the results of a continuous asymptotic analysis of the Euler equations and that one term in the numerical dissipation is removed at low Mach numbers. The same analysis is applied for the first time to a method suggested by Thornber et al. [18] and allows to better explain the behavior of that method. The main difference between these two methods is that $L^2$Roe modifies only the dissipation term in the numerical flux functions, whereas the other method modifies the evaluation of the physical fluxes as well, to no visible benefit.

Numerical results then show that the modification does not destroy the good properties of the original methods over a wide range of test cases. No stability problems are observed. For the case of decaying isotropic turbulence on hexahedral meshes, $L^2$Roe and the method of Thornber et al. perform dramatically better than LMRoe and Roe with $L^2$Roe performing best, confirming the results of the asymptotic analysis.

The additional dissipation observed over the higher wave number range on the tetrahedral mesh

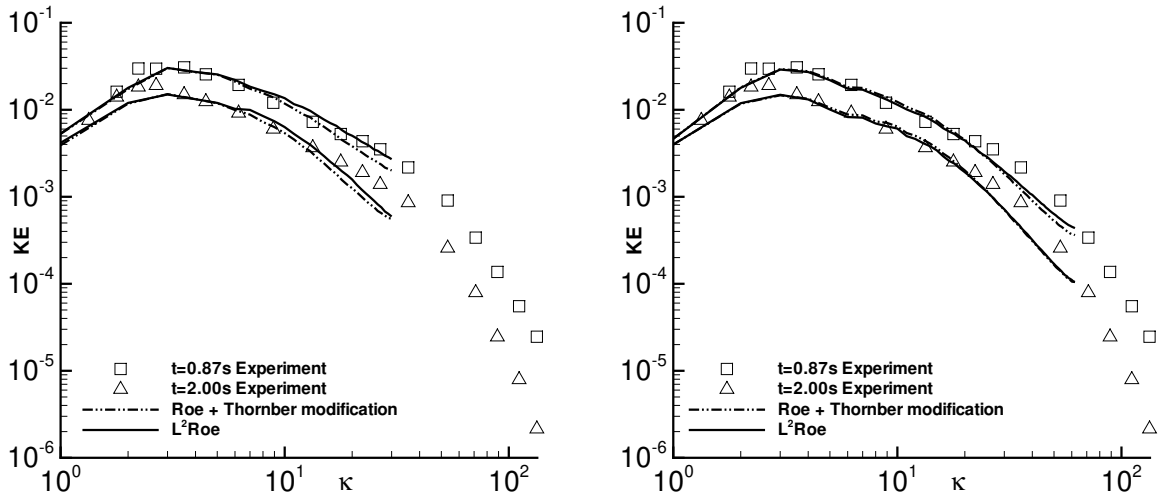


Figure 7: Turbulent kinetic energy spectra at $t = 0.87\,\mathrm{s}$ and $t = 2\,\mathrm{s}$ in the case of decaying isotropic turbulence on a $64^3$ (left) and $128^3$ (right) hexahedral grid; experimental data taken from Comte-Bellot and Corrsin [3].

is not fully understood and is a subject for further investigation.

## Acknowledgement

Financial support has been provided by the German Research Foundation (Deutsche Forschungsgemeinschaft – DFG) in the framework of the Sonderforschungsbereich Transregio 30, project C2, as well as in the framework of the Sonderforschungsbereich Transregio 40, project B5.

## References

[1] P. Birken, *Numerical Methods for the Unsteady Compressible Navier-Stokes Equations*, Habilitation Thesis, University of Kassel, 2012.

[2] P. Birken and A. Meister, *Stability of Preconditioned Finite Volume Schemes at Low Mach Numbers*, BIT, 45(3) (2005).

[3] G. Comte-Bellot and S. Corrsin, *Simple Eulerian time correlation of full- and narrow-band velocity signals in grid generated, isotropic turbulence*, Journal of Fluid Mechanics, 48 (1971), pp. 273–337.

[4] S. Dellacherie, *Analysis of Godunov type schemes applied to the compressible Euler system at low Mach number*, J. Comp. Phys., 229 (2010), pp. 978–1016.

[5] W. George, *The decay of homogeneous isotropic turbulence*, Phys. Fluids A, 4(7) (1992), pp. 1492–1509.

[6] T. Gerhold, O. Friedrich, J. Evans, and M. Galle, *Calculation of Complex Three-Dimensional Configurations Employing the DLR-TAU-Code*, AIAA Paper, 97-0167 (1997).

[7] H. Guillard and A. Murrone, *On the behavior of upwind schemes in the low Mach number limit: II. Godunov type schemes*, Computers & Fluids, 33 (2004), pp. 655–675.

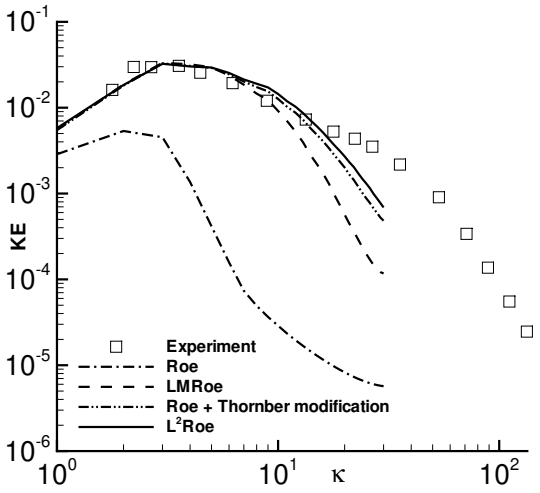


Figure 8: Turbulent kinetic energy spectra at $t = 0.87\,\mathrm{s}$ in the case of decaying isotropic turbulence on a $64^3$ tetrahedral grid; experimental data taken from Comte-Bellot and Corrsin [3];


[8] H. Guillard and C. Viozat, *On the Behaviour of Upwind Schemes in the Low Mach Number Limit*, Computers & Fluids, 28 (1999), pp. 63–86.

[9] W. Haase, M. Braza, and A. R. (Eds., *DESider - A European Effort on Hybrid RANS-LES Modelling, Results of the European-Union Funded Project, 2004-2007*. Series: Notes on Numerical Fluid Mechanics and Multidisciplinary Design, Vol. 103, 2009.

[10] M.-S. Liou, *Mass Flux Schemes and Connection to Shock Instability*, Journal of Computational Physics, 160 (2000), pp. 623–648.

[11] F. Rieper, *A low-Mach number fix for Roe's approximate Riemann solver*, Journal of Computational Physics, 230 (2011), pp. 5263–5287.

[12] F. Rieper and G. Bader, *Influence of cell geometry on the accuracy of upwind schemes in the low Mach number regime*, J. Comp. Phys., 228 (2009), pp. 2918–2933.

[13] M. Shur, P. Spalart, M. Strelets, and A. Travin, *A hybrid RANS-LES approach with delayed-DES and wall-modelled LES capabilities*, International Journal of Heat and Fluid Flow, 29 (2008), pp. 1638–1649.

[14] P. Spalart and S. Allmaras, *A one-equation turbulence model for aerodynamic flows*. Recherche Aérospatiale 1, 1994.

[15] P. Spalart, W.-H. Jou, M. Strelets, and S. Allmaras, *Comments on the Feasibility of LES for Wings and on the Hybrid RANS/LES Approach*. Advances in DNS/LES, Proceedings of the First AFOSR International Conference on DNS/LES, 1997.

[16] M. Strelets, *Detached Eddy Simulation of Massively Separated Flows*, AIAA Paper 2001–0879, 2001.

[17] B. Thornber, D. Drikakis, and D. Youngs, *On entropy generation and dissipation of kinetic energy in high-resolution shock-capturing schemes*, J. Comp. Phys., 227 (2008), pp. 4853–4872.

[18] B. Thornber, A. Mosedale, D. Drikakis, D. Youngs, and R. Williams, *An improved reconstruction method for compressible flows with low Mach number features*, J. Comp. Phys., 227 (2008), pp. 4873–4894.

[19] E. Toro, *Riemann Solvers and Numerical Methods for Fluid Dynamics*, Springer, 1997.

[20] Y. Wada and M.-S. Liou, *A Flux Splitting Scheme With High-Resolution and Robustness for Discontinuities*, AIAA-94-0083, NASA Technical Memorandum 106452, 1994.